The Astrophysical Journal, 941:40 (11pp), 2022 December 10 https://doi.org/10.3847/1538-4357/ac9f35

Structure and Spectroscopic Signatures of Interstellar Sodium Isocyanate Isomers

Miguel Sanz-Novo[1,2], Pablo Ortega[3], Pilar Redondo[1], Antonio Largo[1], José Luis Alonso[2], and Carmen Barrientos[1]
[1] Computational Chemistry Group, Departamento de Química Física y Química Inorgánica, Facultad de Ciencias, Universidad de Valladolid, E-47011 Valladolid, Spain; miguel.sanz.novo@uva.es
[2] Grupo de Espectroscopía Molecular (GEM), Edificio Quifima, Área de Química-Física, Laboratorios de Espectroscopía y Bioespectroscopía, Parque Científico UVa, Unidad Asociada CSIC, E-47011 Valladolid, Spain
[3] Departamento de Química-Física, University of Salamanca, Salamanca E-37008, Spain
Received 2022 September 16; revised 2022 October 27; accepted 2022 October 28; published 2022 December 12

Abstract

The investigation of metal-containing interstellar molecules stands as a prolific field for current astrochemical research. However, the search for many of these systems in the interstellar medium has remained inaccessible to date due to the lack of preliminary spectroscopic data. In this context, pioneering theoretical studies have inspired quantum chemists to study new appealing candidates to enable their subsequent search in space. The aim of this study is to provide high-level theoretical spectroscopic signatures of the tetratomic system [Na, N, C, O]. We have performed a thorough exploration of its potential energy surface employing different state-of-the-art quantum chemical methods and nine different species have been characterized. Moreover, we have evaluated the stability of the most stable isomers against dissociation and explored their main isomerization processes. We therefore suggest sodium isocyanate (NaNCO,$^1\Sigma$) and sodium cyanate, (NaOCN, $^1\Sigma$) as the most relevant candidates for laboratory and interstellar detection. To aid in their eventual spectral search by means of rotational spectroscopy, we report a complete set of the required spectroscopic parameters including the nuclear quadrupole coupling constants, which are needed to interpret their complex hyperfine structure. NaNCO and NaOCN present exceptionally high values of the electric dipole moment (11.4 and 13.6 Debyes, respectively at the CCSD(T,rw)/aug-cc-pVTZ level), which strongly support to perform an eventual radio astronomical search. Furthermore, both isomers exhibit rather small vibrational frequencies, which indicates that these species are certainly floppy molecules.

Unified Astronomy Thesaurus concepts: Astrochemistry (75); Interstellar medium (847); Molecular data (2259); Computational methods (1965)

1. Introduction

The molecular inventory of metal-bearing species (in the chemist's sense) detected so far in the interstellar medium (ISM) comprises almost thirty species, highlighting the families of metal halides (NaCl, AlCl, KCl, and AlF, Cernicharo & Guélin 1987), metal cyanides and isocyanides (MgNC; Guélin et al. 1993; Kawaguchi et al. 1993, MgCN; Ziurys et al. 1995, SiCN; Guélin et al. 2000, NaCN; Turner et al. 1994; Highberger et al. 2001, AlNC; Ziurys et al. 2002, SiNC; Guélin et al. 2004, KCN; Pulliam et al. 2010, FeCN; Zack et al. 2011, CaNC; Cernicharo et al. 2019a), HMgNC; Cabezas et al. 2013, and MgC_3N, Cernicharo et al. 2019b). Most of these molecules have been found toward the carbon-rich mass-losing star IRC+10216, remarking this astronomical source as an extraordinary target to search for related systems. Within this framework, Pardo et al. (2021b) have carried out deep observations using the Yebes 40 m radio telescope, updating the older spectral survey available for this source in the *Q* band (Kawaguchi et al. 1995).

In the last couple of years, the astrophysical community has made great efforts to disentangle the vast amount of new and very sensitive astronomical data, such as that provided by the Green Bank Telescope (GBT) GOTHAM survey (McGuire et al. 2020), the Yebes 40 m QUIJOTE line survey (Cernicharo et al. 2021) and the Yebes 40 m survey toward G+0.693-0.027 (Rivilla et al. 2021). However, deciphering these new observational data sets stands as a very puzzling task. Hence, in order to guide laboratory spectral searches and, more importantly, to facilitate interstellar identifications, purely theoretical studies are lately helping to fill the gap between laboratory (terrestrial) and radio astronomical data.

In this context, hydrometal cyanide and isocyanide molecules have received considerable attention from both experimental (HSiCN/HSiNC; Sanz et al. 2002, HZnCN; Sun et al. 2009, HMgCN; Cabezas et al. 2013) and theoretical (HZnCN/HZnNC; Redondo et al. 2015, HFeCN/HFeNC; Redondo et al. 2016, HTiCN/HTiNC; Redondo et al. 2019, HCaCN/HCaNC; Redondo et al. 2020 and HAlCN/HAlNC; Redondo et al. 2022) point of view aiming to help an eventual interstellar detection. Nevertheless, there is limited theoretical or laboratory data for metal-isocyanates and metal-cyanates that aid their characterization in space, which is required to elucidate their role in interstellar chemistry. Aside from a few outdated theoretical studies on HBeNCO (Pasinszki et al. 1993), LiNCO (Rode et al. 1972; Poppinger & Radom 1978), and CaNCO (Ellingboe et al. 1986), it should be highlighted the theoretical investigation of tetratomic isomers comprising Al, N, C, and O atoms (Trabelsi et al. 2019), where the linear aluminum isocyanate (AlNCO) was found to be the most stable isomer at the CCSD(T)/CBS level. Additionally, high-level ab initio spectroscopic predictions have been recently reported on the electronic structures and spectroscopic parameters of the related MgNCO (Vega-Vega et al. 2017) and HMgNCO (Bai & Yu 2022). Concerning Na-isocyanates and cyanates, besides a preliminary study reported almost 20 yr ago (Veszprémi et al. 1994), to the best of our knowledge, there is no experimental or theoretical information available for the [Na, N, C, O] system.

Moreover, the study of peptide-bond-bearing molecules, i.e., molecules containing the NCO backbone, is of paramount relevance for astrochemists and has been deeply ingrained in understanding the evolution of prebiotic chemistry. These molecules are branded as "building blocks of life" since they can participate in the amide linkage of amino acids to form polypeptide chains and, subsequently, proteins (Pascal et al. 2005). Therefore, their observation in the interstellar medium (ISM) can provide important hints on the primal chemical steps in the formation of prebiotic molecules and shall ultimately help us rationalize the origin of life on a primitive Earth.

This peptide-type bond is present in several interstellar complex organic molecules (iCOMs see Colzi et al. 2021 and also McGuire 2018 for a census), such as formamide ($HC(O)NH_2$; Halfen et al. 2015; Cernicharo et al. 2016; Ligterink et al. 2017; Martín-Doménech et al. 2017; Ligterink et al. 2017; Csengeri et al. 2019; Gorai et al. 2020; Manigand et al. 2020; Colzi et al. 2021; Ligterink et al. 2021), acetamide ($CH_3C(O)NH_2$; Hollis et al. 2006, Halfen et al. 2015, Cernicharo et al. 2016; Belloche et al. 2017; Ligterink et al. 2020, 2022; Colzi et al. 2021), N-methylformamide (CH_3NHCHO; Belloche et al. 2017, 2019; Ligterink et al. 2020; Colzi et al. 2021) and urea ($NH_2C(O)NH2$; Belloche et al. 2019; Jiménez-Serra et al. 2020). Nevertheless, among all iCOMs, only four species contain the so-called isocyanate (-N=C=O) functional group. Since the first interstellar detection of isocyanic acid toward Sgr B2 (OH) in the early 1970 s (HNCO; Snyder & Buhl 1972), this molecule has been identified in diverse astronomical sources (Jackson et al. 1984; Nguyen-Q-Rieu et al. 1991; Helmich & van Dishoeck 1997; Turner et al. 1999; Bisschop et al. 2007; Rodríguez-Fernández et al. 2010; Zeng et al. 2018; Nazari et al. 2021; Canelo et al. 2021), highlighting a very recent detection in the disk of our galaxy, outside the Galactic center (Colzi et al. 2021). Its cationic form, H_2NCO^+, was tentatively identified in the PRIMOS spectral line survey of Sgr B2(N) (Gupta et al. 2013) and, more recently, it was conclusively detected through millimeter emission transitions toward the dense core L483 together with the elusive NCO radical (Marcelino et al. 2018), the simplest molecule containing the backbone of the peptide bond. Additionally, their rational step up in complexity, methylisocyanate (CH_3NCO; Halfen et al. 2015; Cernicharo et al. 2016; Ligterink et al. 2017; Martín-Doménech et al. 2017, Ligterink et al. 2017, Csengeri et al. 2019; Gorai et al. 2020; Manigand et al. 2020; Colzi et al. 2021; Ligterink et al. 2021) and ethyl isocyanate (CH_3CH_2NCO; Rodríguez-Almeida et al. 2021) have also been found in the ISM. However, metal-isocyanates remain undetected both in the laboratory and in space. This fact further motivates quantum chemists to provide accurate theoretical spectroscopic data.

In this work, we report a state-of-the-art theoretical study on the electronic structure and spectroscopy of the tetratomic [Na, N, C, O] molecular system. Hence, we explored its ground-state potential energy surface (PES) to unveil the most expected candidates for laboratory and interstellar detection. In this context, we performed a thorough analysis of the interconversion and fragmentation processes between isomers aiming to enlighten the stability of these molecules in the ISM. Moreover, we provide a high-level calculated array of rotational spectroscopic constants for the most stable systems, NaNCO and NaOCN, which shall be used to conduct spectral searches and serve as relevant benchmark data to compare against experimental information once available. Moreover, this information should shed light on interstellar heavy-metal chemistry and refine theoretical astrochemical networks that involve these elements.

2. Quantum Chemical Methodology

We first explored the singlet and triplet potential energy surface (PES) of the [Na, N, C, O] system in the framework of the density functional theory (DFT), hunting for the fundamental states of the plausible stationary points. Then, geometries of the energy minima and transition states were initially optimized using the double-hybrid B2PLYP functional (Grimme 2006) combined with Grimme's DFT-D3 empirical dispersion term (B2PLYPD3, Schwabe & Grimme 2007). This function adds nonlocal electron correlation effects to a standard hybrid functional by second-order perturbation theory and has been proved to properly estimate experimental rotational spectroscopic parameters (Sanz-Novo et al. 2020). Additional geometric optimizations were performed at the ab initio coupled-cluster CCSD(T,rw) and CCSD(T,all) levels, where the "rw" and "all" specifies the inclusion of the 2 s and 2p inner shells of Na in the correlation calculation or the inclusion of all electrons, respectively. It includes single and double excitations as well as triple excitations through a perturbative treatment (Raghavachari et al. 1989). Coupled-cluster (CC) theory has been established as a suitable methodology to provide reasonably accurate spectroscopic parameters and has been extensively used to correctly reproduce the molecular geometry for different metal-bearing species (e.g., Cernicharo et al. 2019b). For both DFT and ab initio calculations, we employed Dunning's correlation-consistent triple-zeta (aug-cc-pVTZ) and quadruple-zeta (aug-cc-pVQZ) basis set (Dunning 1989; Woon & Dunning 1993) including both polarization and diffuse functions on all elements. What is more, we also employed the "weighted sets" correlation-consistent basis sets for core correlation, cc-pwCVQZ and aug-cc-pwCVQZ basis set, a Gaussian basis set which is of special interest for accurate calculations of the spectroscopic properties of molecules containing alkali metal (K-Fr) and alkaline earth (Ca-Ra) elements (Hill & Peterson 2017). Additionally, for comparison purposes, we carried out geometry optimizations at the explicitly correlated coupled-cluster CCSD(T,rw)-F12 level (Knizia et al. 2009) employing the cc-pVTZ-F12 and cc-pVQZ-F12 basis set (Peterson et al. 2008).

Afterward, for each optimized structure, we computed harmonic vibrational frequencies to identify the stationary points as true minima (all their frequencies are real) or transition states (one frequency is imaginary) and estimate the zero-point vibrational energies (ZPVEs) at the same level of theory as that employed for the geometry optimization. Moreover, transition states have been verified by performing intrinsic reaction coordinate (IRC) computations (Gonzalez & Schlegel 1989, 1990), when available, and also by checking the vibrational imaginary frequency.

To enhance the prediction of the IR spectra for the two most stable isomers, NaNCO and NaOCN, we computed anharmonic corrections at the CCSD(T,rw)/aug-cc-pVTZ level using the second-order vibrational perturbation theory (VPT2; Mills 1972; Barone 2005). Moreover, this information should be of interest to adequately estimate the vibrational contribution (Q_v) to the total partition function (Q_{tot}), which is required to

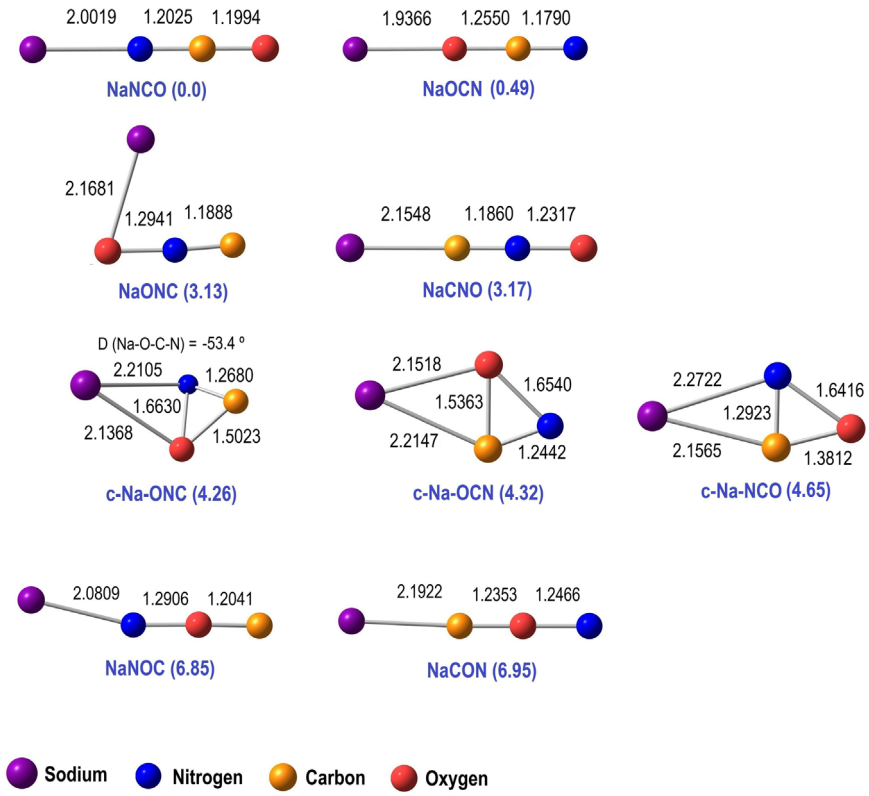

Figure 1. Optimized structures at the CCSD(T,rw)/aug-cc-pVTZ level for the [Na, N, C, O] isomers (except for the higher-in-energy NaNOC and NaCON, which are optimized at the B2PLYPD3/aug-cc-pVQZ level). Energies are given in eV while bond distances are given in angstroms.

achieve a proper estimation of the total column density (upper limit) of a molecule.

We have also computed the T1 diagnostic (Lee & Taylor 1989) to prove the suitability of our single reference computations. We found values of 0.0145 and 0.0136 at the CCSD(T,rw)-F12/cc-pCVQZ-F12 level for the two most stable species (NaNCO and NaOCN), respectively, which indicates the usefulness of the CCSD(T) method to characterize the electronic structure of these molecules. Moreover, we carried out complete active space multiconfiguration self-consistent field (CASSCF; Werner & Knowles 1985a, 1985b) computations. We obtained c_0^2 values of 0.921 and 0.918 for NaNCO and NaOCN, respectively, which are greater than 0.90 (Jiang et al. 2012), further corroborating that both molecules do not exhibit significant multireference character.

To perform all quantum calculations, we employed the GAUSSIAN 16 (Frisch et al. 2016), CFOUR (Stanton et al. 2013), and MOLPRO (Werner et al. 2019) suites of programs.

3. Results and Discussion

3.1. Isomeric Panorama, Energetics, and Structure

We have searched for all the possible structures of molecular formula [Na, N, C, O], including linear, bent, and three-membered ring (cyclic) arrangements. The CCSD(T,rw)/aug-cc-pVTZ optimized geometries for the different isomers are depicted in Figure 1. As shown, nine true energy minima have been characterized in their lowest-lying singlet state. The corresponding triplet states were found much higher in energy (>5 eV) and, therefore, they are not included in the present results.

According to our computations, sodium isocyanate, NaNCO ($^1\Sigma$), is the most stable [Na, N, C, O] isomer, in good agreement with previous experimental results reported on related isocyanates (Poppinger & Radom 1978). The corresponding cyanate counterpart, NaOCN ($^1\Sigma$), is located at 11.4 kcal mol^{-1} (0.49 eV or 5686 K) at the CCSD(T,rw)/aug-cc-pVTZ level above the global minimum. Following in energy, we found NaCNO ($^1\Sigma$), named sodium fulminate, which lies at 73.1 kcal mol^{-1} (3.17 eV or 36786 K) (CCSD(T,rw)/aug-cc-pVTZ level). When the interaction takes place between the sodium atom and, exclusively, the oxygen atom of the CNO unit, a slightly more stable bent structure than NaNCO, namely sodium isofulminate, NaONC (A'), is obtained, which lies at 72.2 kcal mol^{-1} (3.13 eV or 36322 K at the CCSD(T,rw) level). We also found three higher-in-energy cyclic structures, c-Na-ONC (^{1}A), c-Na-OCN (^{1}A), and c-Na-NCO (^{1}A), which arise from the interaction between the sodium atom and ON, CO, CN bonds of the cyclic c-NCO unit, respectively. These isomers are located at 98.3 (4.26), 99.7 (4.32), and 107.2 (4.65) kcal mol^{-1} (eV), respectively, with respect to NaNCO. Moreover, for c-Na-ONC, the carbon atom is to some extent involved in the bonding, yielding to a nonplanar structure. Finally, two additional and very high-energy quasilinear isomers, NaNOC and NaCON, located more than 150 kcal mol^{-1} (6.5 eV or 75480 K) above the global minimum were initially considered; they were lastly discarded in a subsequent screening. This marked instability can be straightforwardly attributed to the presence of the particularly labile NOC moiety.

Moreover, we refined the geometry and energetic computations regarding the two most stable species at the CCSD(T,all)/cc-pwCVQZ, CCSD(T,all)/aug-cc-pwCVQZ and CCSD(T,

Table 1
Relative Energies, Including Zero-point Corrections in Kcal/mol and eV (in Parenthesis) for the [Na, N, C, O] Isomers Computed at Different Levels of Theory

Isomer	B2PLYPD3/aug-cc-pVQZ	CCSD(T,rw)/aug-cc-pVTZ	CCSD(T,all)/cc-pwCVQZ	CCSD(T,all)/aug-cc-pwCVQZ	CCSD(T,rw)-F12/cc-pCVTZ-F12	CCSD(T,rw)-F12/cc-pCVQZ-F12
NaNCO ($^1\Sigma$)	0.0 (0.00)	0.0 (0.00)	0.0(0.00)	0.0(0.00)	0.0 (0.00)	0.0 (0.00)
NaOCN ($^1\Sigma$)	12.0 (0.52)	11.4 (0.49)	10.3(0.45)	10.4(0.45)	10.6 (0.46)	10.6 (0.46)
NaCNO ($^1\Sigma$)	72.9 (3.16)	73.1 (3.17)		…	…	…
NaONC (A′)	74.2 (3.22)	72.2 (3.13)		…	…	…
c-Na-ONC (^{1}A)	103.1 (4.47)	98.3 (4.26)		…	…	…
c-Na-OCN (^{1}A)	103.8 (4.50)	99.7 (4.32)		…	…	…
c-Na-NCO (^{1}A)	111.6 (4.84)	107.2 (4.65)		…	…	…
NaNOC	158.0 (6.85)	…		…	…	…
NaCON	160.3 (6.95)	…		…	…	…

Note. [a] ZPVEs are computed at the same level employed for the optimizations except for the CCSD(T,all)/aug-cc-pwCVQZ level, where ZPVEs are computed at the CCSD(T,all)/cc-pwCVQZ level.

rw)-F12/cc-pVTZ-F12 levels. To validate the theoretical methodology employed in the present work, we carried out computations at different levels of theory for the related c-NaNC (^{1}A′) system (see Table A1 for detailed information). We then compared our theoretical results with the experimentally determined structural parameters from a previous high-resolution molecular beam study (Van Vaals et al. 1984) and observed an outstanding resemblance when the CCSD(T,all)/aug-cc-pwCVQZ level is used (Root Mean Square deviation, rms, of ∼0.008). Therefore, although the CCSD(T,all)/aug-cc-pwCVQZ, CCSD(T,rw)-F12/cc-pVTZ-F12, CCSD(T,rw)-F12/cc-pVQZ-F12 levels also provide good results, we will select the CCSD(T,all)/aug-cc-pwCVQZ as the best methodology to obtain a trustworthy geometry for the most relevant isomers, which will be used later on in Section 3.3 to derive the desired spectroscopic properties.

In Table 1 we collect the relative energies for the [Na, C, N, O] isomers, with respect to the most stable isomer (NaNCO, $^1\Sigma$), which are calculated at different levels of theory (see Section 2). It should be noted that regardless of the computational level, the stability order remains unchanged, excluding NaCNO ($^1\Sigma$) and NaONC (A'), whose stability order is inverted when employing CC methodologies. At all levels of theory, both sodium isocyanate (NaNCO, $^1\Sigma$) and sodium cyanate (NaOCN, $^1\Sigma$) isomers appear as the most stable species. The energy difference between them computed at the CCSD(T,all)/aug-cc-pwCVQZ level (10.4 kcal mol^{-1}) is very close to that computed using the explicitly correlated coupled-cluster CCSD(T,rw)- method (10.6 kcal mol^{-1})in conjunction with both cc-pCVTZ and cc-pCVQZ-F12 basis sets. The inclusion of diffuse functions on the cc-pwCVQZ basis set does not practically change the relative energy between the two more stable isomers (see Table 2). Furthermore, a significant leap in the relative stability of more than 60 kcal mol^{-1} (2.6 eV or 30200 K) is observed while moving to the higher-in-energy isomers. The same stability trend was found for the related [H, N, C, O] system, with isocyanic acid (HNCO) as the global minimum in energy. Its metastable isomers cyanic acid (HOCN) and fulminic acid (HCNO), which have also been detected in the ISM (Marcelino et al. 2009; Brünken et al. 2010), are located at 24.3 kcal mol^{-1} (1.05 eV or 12214 K) and 70.2 kcal mol^{-1} (3.05 eV or 35334 K), respectively, above HNCO (computed at the CCSD(T)/cc-pVQZ level for the so-called planar structures, Mladenovic & Lewerenz 2008). Therefore, HNCO and HOCN are found at rather similar relative energies compared to their sodium analogs, sodium cyanate (0.49 eV at the CCSD(T,rw)/aug-cc-pVTZ level) and sodium fulminate (3.17 eV at the CCSD(T,rw)/aug-cc-pVTZ level).

Additionally, we can also compare our results against previous theoretical information reported on other metal-cyanates and isocyanates (e.g., M = Li, Mg, and Al). First, the predicted isomeric landscape of NaNCO is significantly richer than that shown for LiNCO (Poppinger & Radom 1978), where no cyclic structures were initially considered. Regarding magnesium isocyanate (MgNCO), its cyanate isomer, MgOCN, lies at 15.8 kcal mol^{-1} (0.68 eV) at the CCSD(T)/aug-cc-pVTZ level (Vega-Vega et al. 2017) with respect to MgNCO. Finally, in a recent investigation reported on the [Al, N, C, O] system (Trabelsi et al. 2019), a quasilinear cyanate isomer AlOCN was located at 16.6 kcal mol (0.72 eV) at the CCSD(T)/CBS level of theory with respect to its isocyanate counterpart. These energetic differences bear a reasonably close resemblance to those presented in the current investigation, and further suggest both sodium cyanate and sodium isocyanate as appealing candidates for laboratory and astronomical detection. Consequently, NaNCO and NaOCN will be the main focus of our spectroscopic predictions (see Section 3.3).

Afterward, the structural parameters of the four most stable [Na, N, C, O] isomers (computed at different levels of theory) are presented in Table 2. At first sight, slightly smaller values of the Na–X (X = N, O, C) bond are obtained at the CCSD(T, rw) level compared to those DFT predicted. Nevertheless, we observe an overall good agreement among the computed structural parameters despite the different levels of theory. The most stable isomer, NaNCO, exhibits a linear configuration, very similar to those reported for LiNCO (Rode et al. 1972; Poppinger & Radom 1978), MgNCO (Vega-Vega et al. 2017), CaNCO (Ellingboe et al. 1986) and AlNCO (Trabelsi et al. 2019). Additionally, as seen in Table 3, the inclusion of diffuse functions does not modify significantly the resulting geometry. What is more, both NaNCO and NaOCN isomers can be understood as the result of the substitution of the hydrogen atom in either isocyanic or cyanic acid, respectively, by a sodium atom. This substitution results in a shortening of the r (N–C) and r(C–O) bond distances compared to the corresponding experimentally determined bond lengths for HNCO [r

Table 2
Structural Parameters for the [Na, N, C, O] Isomers Below 4.3 eV (100 kcal mol^{-1}) Computed at Different Levels of Theory

Isomer	Parameter[a]	B2PLYPD3 /aug-cc-pVQZ	CCSD(T,rw)/aug-cc-pVTZ	CCSD(T,all)/cc-pwCVQZ	CCSD(T,all)/aug-cc-pwCVQZ	CCSD(T,rw)-F12/cc-pCVTZ-F12	CCSD(T,rw)-F12/cc-pCVQZ-F12
NaNCO	r(Na-N)	2.0905	2.0019	2.0766	2.0776	2.0792	2.0778
($^1\Sigma$)	r(N-C)	1.1970	1.2025	1.1958	1.1959	1.1981	1.1978
	r(C-O)	1.1952	1.1994	1.1930	1.1943	1.196	1.1957
NaOCN	r(Na-O)	2.0107	1.9366	1.9885	1.9891	1.9909	1.9893
($^1\Sigma$)	r(O-C)	1.2482	1.2550	1.2501	1.2498	1.2514	1.2512
	r(C-N)	1.1742	1.1790	1.1719	1.1729	1.1752	1.1749
NaCNO	r(Na-C)	2.2197	2.1548	…	…		…
($^1\Sigma$)	r(C-N)	1.1829	1.1860	…	…		…
	r(N-O)	1.2232	1.2317	…	…		…
NaONC	r(Na-O)	2.2418	2.1681	…	…		…
(A′)	r(O-N)	1.2851	1.2941	…	…		…
	r(N-C)	1.1846	1.1888	…	…		…
	∠(Na-O-N)	74.4	72.8	…	…		…
	∠(O-N.C)	172.2	173.3	…	…		…

Note.
[a] Bond distances are given in angstroms and angles are given in degrees.

Table 3
Dissociation Energies (D_0), in kcal mol^{-1} (eV), Computed at the B2PLYPD3/aug-cc-pVQZ Level of Theory

Reaction	B2PLYPD3
NaNCO → Na + NCO	92.7 (4.02)
NaNCO → NaN + CO	171.8 (7.45)
NaOCN → Na + NCO	80.6 (3.50)
NaOCN → NaO + CN	155.1 (6.72)
NaONC → NaO + CN	92.9 (4.03)
NaONC → Na + CNO	81.2 (3.52)
NaCNO → Na + CNO	82.6 (3.58)

Note. (a) Zero-point vibrational energy corrections are included, which are computed at the same level of theory.

(N–C) = 1.2140 Å, and r(C–O) = 1.1664 Å, Yamada 1980]. However, the Na-bearing structures are significantly different from those belonging to the [H, N, C, O] system, which presents in all cases clearly bent configurations.

Finally, when we make a comparison of the C–N bond distances within the four most stable isomers (see Figure 1), we spot a significantly larger bond length for NaNCO (1.2025 Å). This fact can be rationalized in terms of the bonding of the sodium atom to the CN moiety through the nitrogen atom, which weakens the C–N bond. This behavior was also detected in previous works on metal hydrides (M = Zn, Fe, Ti, and Ca, Redondo et al. 2015, 2016, 2019, 2020).

3.2. Isomerization and Fragmentation Processes

Once we have identified and described the different [Na, N, C, O] isomers, we then analyzed the isomerization processes between them. In Figure 2 we depict the energy profiles computed at the B2PLYPD3/aug-cc-pVQZ level. Transition states are denoted as TS, followed by a cardinal number related to the stability order. As can be seen in Figure 2, the two most stable isomers, NaNCO and NaOCN, are connected through TS1; this process presents a low barrier of 0.9 kcal mol^{-1} (0.04 eV or 453 K). Given the small value found for the interconversion process between the two more stable isomers, we have performed a calculation at the CCSD(T,rw)-F12/cc-pCVTZ-F12 level, obtaining a value of only 0.13 kcal mol^{-1} (65 K). This small barrier suggests that NaOCN can easily interconvert into NaNCO however, both isomers could be present in the cold regions of the ISM. On the other hand, it should be noted that TS1 is characterized by a small imaginary frequency (38i cm^{-1} at the CCSD(T,rw)-F12/cc-pCVTZ-F12 level), indicating a very broad barrier. Therefore, NaNCO should be stable against isomerization once formed.

We have also studied isomerization processes involving the less stable cyclic isomers, c-Na-OCN and c-Na-ONC. Regarding the cyclic isomer arising from the interaction of the sodium atom with the CO moiety (c-Na-OCN), its interconversion process to NaOCN comprises TS3, located at 3.5 kcal mol^{-1} (0.15 eV or 1761 K) with respect to c-Na-OCN. On the other hand, the isomerization of c-Na-OCN to NaONC involves TS5, which lies at 7.8 kcal mol^{-1} (0.34 eV or 3925 K) above c-Na-OCN. Additionally, the isomerization of c-Na-ONC to NaOCN takes place through TS4, which lies at 1.6 kcal mol^{-1} (0.07 eV or 805 K) with respect to c-Na-OCN. Finally, the interconversion of NaONC to NaCNO involves TS2, and a relatively small net barrier of 3.1 kcal mol^{-1} (0.13 eV or 1560 K) is calculated. Taken all together, all the interconversion processes between the isomers under study, except for the conversion of NaOCN into NaNCO, involve significant net activation barriers and, therefore, isomerization processes shall not be feasible under the temperature conditions of cold interstellar regions. Thus, our results suggest that if any of these isomers were generated efficiently under interstellar conditions, it is most likely that they could coexist in the ISM.

To obtain meaningful information on the stability of the most stable [Na, C, N, O] isomers in terms of the adiabatic dissociation energies, we have evaluated different dissociation pathways, which can be categorized into two groups: (a) Processes leading to a sodium atom together with an NCO or a CNO unit, and (b) Processes yielding two diatomic fragments. In Table 3 we report the dissociation energies calculated at the B2PLYPD3/aug-cc-pVTZ level. Additionally, the two most stable dissociation products are also included in Figure 2 for comparison. At first glance, all isomers are stable against

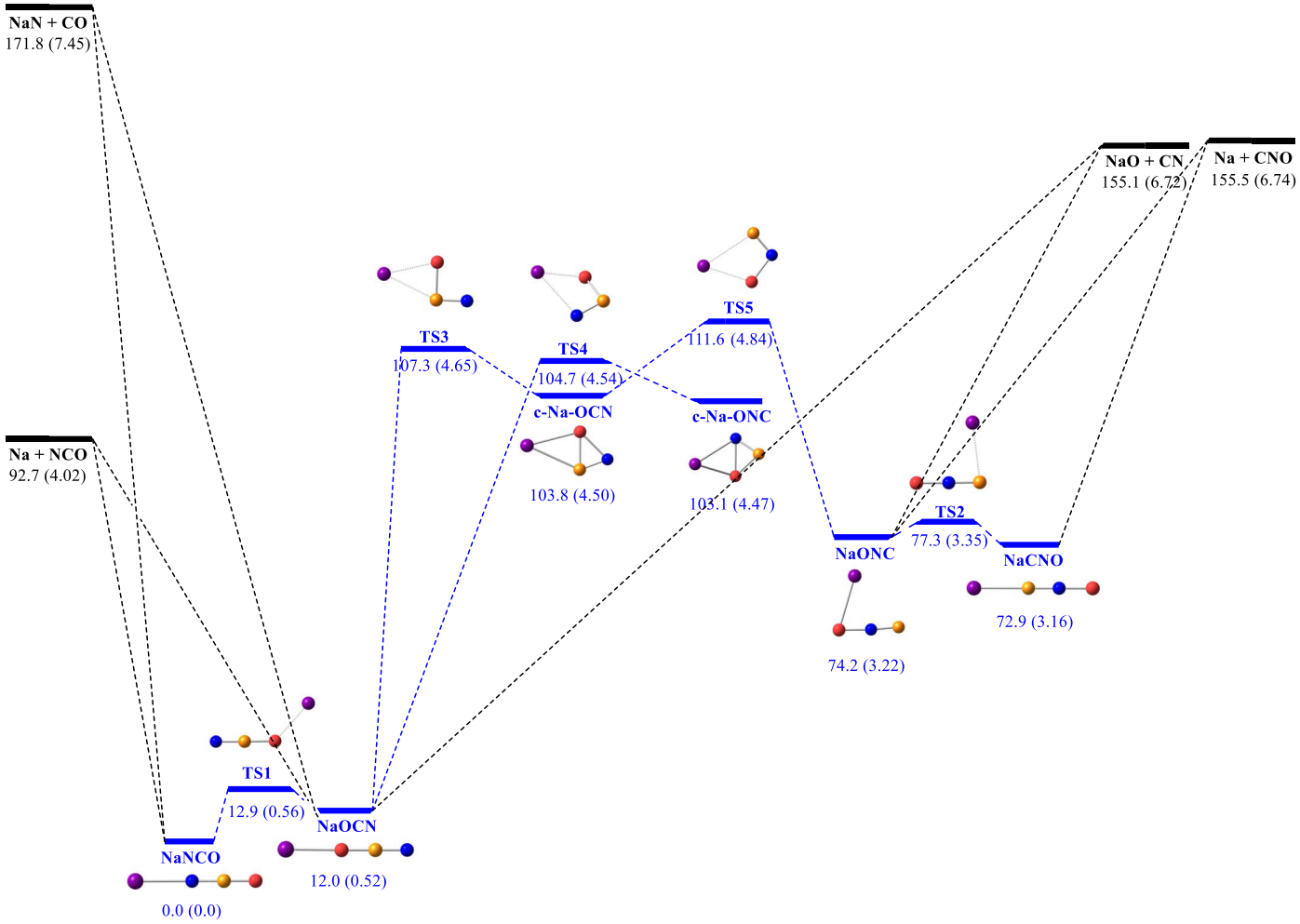

Figure 2. Energy profile for the isomerization process between the most relevant isomers. Relative energies, in kcal mol^{-1} (eV), with respect to NaNCO computed at the B2PLYPD3/aug-cc-pVQZ are given. Plausible dissociation products are also included for comparison (depicted in black).

fragmentation based on the large positive values of the dissociation energies. As shown in Table 3, the dissociation energies corresponding to the generation of Na and NCO from NaNCO and NaOCN are relatively high, 92.7 kcal mol^{-1} (4.02 eV) and 80.6 kcal mol^{-1} (3.50 eV), respectively. Moreover, the dissociation energies of NaNCO and NaOCN to give either NaN + CO or NaO + CN, respectively, are the highest, ranging from 155.1 kcal mol^{-1} (6.72 eV) to 171.8 kcal mol^{-1} (7.45 eV). These results suggest that both isomers are the most stable ones against dissociation, and, consequently, the most relevant species from a laboratory (terrestrial) point of view. Contrariwise, the stability upon dissociation of NaONC and NaCNO to give either the diatomic units NaO + CN or Na + CNO is slightly hampered, and the corresponding dissociation energies vary from 81.2 to 92.9 kcal mol^{-1} (3.52 and 4.03 eV).

Nonetheless, the abovementioned dissociation fragments—and their corresponding ionic and radical forms—can also be conceived as the main precursors of all the [Na, N, C, O] isomers in the gas phase or dust grains, as well as the precursors of all the [H, N, C, O] isomers, which can be generated by radicals NCO and CNO by dissociative recombination processes (Marcelino et al. 2010).

Regarding plausible formation pathways of both NaNCO and NaONC in the ISM and keeping in mind the detection of NaCN (with a T-shape structure) and several O-bearing molecules toward IRC+10216, we can suggest different ion–molecule reactions between NaCN and O-bearing molecules such as OH^+ or OH·. Moreover, H_2NCO^+, the protonated cationic form of HNCO, which was detected toward the dense core L483, can be also considered an interesting precursor of NaNCO isomers. In this framework, we can propose ion–molecule reactions starting with H_2NCO^+ or $HNCO^+$.

Additionally, a different but also quite interesting approach is to suggest the formation of NaNCO and NaOCN in star-forming regions (i.e., in Sgr B2). In this framework, NaOH has been tentatively identified in the molecular cloud Sgr B2 (Hollis & Rhodes 1982) and also in Orion-KL (Turner 1991). We can, therefore, propose NaOH as another appealing precursor of sodium isocyanate and its isomers, which may react with CN· or HCN to form NaNCO or NaOCN.

3.3. Spectroscopic Parameters for Laboratory or Astronomical Detection

In the last couple of years, astrophysicists are starting to employ spectral line surveys as a "conventional" laboratory spectrum in the hunt for new species (Cernicharo et al. 2019b; Pardo et al. 2021a; Cernicharo et al. 2021), and purely theoretical data are being used to achieve conclusive interstellar

Table 4
Theoretical Spectroscopic Constants for the Lowest-in-energy [Na, N, C, O] Isomers

Parameter	NaNCO	NaOCN
B_e[a]	2436.030	2635.215
B_0	2446.767	2636.545
D	0.423	0.441
eQq (^{23}Na)[b]	−11.12	−9.98
eQq (^{14}N)	−0.0342	−2.06
μ[c]	11.4	13.6

Note.
[a] Equilibrium rotational constant (B_e in MHz) computed at the CCSD(T,all)/aug-cc-pwCVQZ, ground vibrational state rotational constant (B_0 in MHz), and centrifugal distortion constants (D in kHz) are computed at the CCSD(T,rw)/aug-cc-pVTZ level. (b) Nuclear quadrupole coupling constants (eQq in MHz) for both ^{23}Na and ^{14}N nuclei computed at the CCSD(rw)/aug-cc-pVTZ. (c) Electric dipole moment (μ in Debyes).

Table 5
Rotational and Vibrational Partition Functions of NaNCO and NaOCN at Typical Temperatures

	NaNCO ($Q_n = 4$)		NaOCN($Q_n = 12$)	
Temperature (K)	Q_r[a]	Q_v[b]	Q_r	Q_v
9.375	320.76	1.00	889.54	1.00
18.75	641.51	1.02	1779.07	1.02
37.50	1283.03	1.22	3558.15	1.26
75.00	2566.05	2.09	7116.29	2.22
150.00	5132.11	5.22	14232.58	5.68
225.00	7698.16	10.79	21348.87	11.93
300.00	10264.22	20.24	28465.16	22.80

Notes.
[a] Q_r is the rotational partition function, which includes hyperfine splittings.
[b] Q_v is the vibrational partition function.

detections. Hence, to facilitate eventual spectral searches, we provide a high-level calculated array of the relevant spectroscopic parameters to rotational spectroscopy for the most stable isomers, NaNCO and NaOCN. In Table 4, the equilibrium and ground-state rotational constants are listed. The latest was calculated by including the vibrational correction, estimated from the vibration–rotation coupling constants (computed from the full anharmonic cubic force field, CFF) and degeneracy factors of the vibrational modes. It should be noted that linear species are relatively easy to find both in the laboratory and in the ISM due to their characteristic spacing of approximately $\sim 2B$ in the rotational spectra. However, while going to higher frequencies, centrifugal distortion constants are mandatory to correctly reproduce the spectrum (i.e., in the millimeter-wave region). Thus, centrifugal distortion constants are also presented in Table 4. Moreover, we observe exceptionally high values of the electric dipole moments ($\mu_{\rm NaNCO} = 11.4$ D and $\mu_{\rm NaOCN} = 13.6$ D, respectively), which strongly suggest that both species, if present in the gas phase, should be detectable in the ISM by analyzing their radio astronomical features.

It is well known that for low-frequency surveys, i.e., those conducted at centimeter wavelengths with telescopes such as the Yebes 40 m and the Green Bank Telescope (GBT), reliable predictions of the hyperfine structure can help the robust identification of interstellar molecules (McCarthy & McGuire 2021). For instance, the scrutiny of the hyperfine structure of N-protonated isocyanic acid (H_2NCO^+) was essential for its proper line-by-line identification toward the molecular cloud G+0693-0.027 (Rodríguez-Almeida et al. 2021). In this context, both NaNCO and NaOCN exhibit two distinct nuclei with quadrupole moment, ^{23}Na ($I = 3/2$) and ^{14}N ($I = 1$), which interact with the electric field gradient created by the rest of the molecule at each nucleus. Thus, their rotational levels are split, leading to a significantly complex hyperfine structure. To aid in the assignment and interpretation of the rotational spectra, we computed the ^{23}Na and ^{14}N nuclear quadrupole coupling constants (eQq) for both isomers at the CCSD(rw)/aug-cc-pVTZ level. It should be noted that for NaNCO, the value of the ^{14}N nuclear quadrupole coupling constant, (eQq (^{14}N) = −0.0342 MHz), is very low (about ~ 3 orders of magnitude smaller than that attributable to the ^{23}Na nucleus) and, therefore, the corresponding coupling effect should be almost imperceptible in the rotational spectra (splittings of very few kHz are expected), even if a cavity-based technique is used (Cabezas et al. 2014). Thus, it has not been taken into account in the rotational spectra simulations of NaNCO or in the computation of the corresponding rotational partition function (see below).

Additionally, for astronomical purposes, in Table 5 we provide the values of the rotational (Q_r) and vibrational (Q_v) partition functions of NaNCO and NaOCN at various temperatures. We employed the theoretically predicted rotational constant to calculate the values of Q_r from first principles at typical temperatures, as applied in the Jet Propulsion Laboratory (JPL) database (Pickett et al. 1998). Furthermore, the values of (Q_r) are multiplied by the nuclear spin statics contribution [i.e., $Q_n = (2I_{\rm Na}+1) = 4$ for NaNCO and $Q_{\rm n} = (2I_N+1)\,(2I_{\rm Na}+1) = 12$, due to the presence of ^{14}N and ^{23}Na nuclei for NaOCN], which should be of interest for predictions in the Q-band. Then, we estimated the vibrational part, Q_v, using Equation (3).60 of Gordy & Cook (1984) and CCSD (T, rw) frequency computations, including anharmonic contributions (detailed information is given in Section 2), where all the vibrational modes were taken into account (see Table 6). The total partition function, $Q_{\rm tot}$ can be therefore calculated as the product of Q_r and Q_v.

To aid future spectral searches, we have used the SPCAT program (Pickett 1991) to simulate the rotational spectrum for both isomers up to 50 GHz from the computed high-level parameters presented in Table 4. Their predicted synthetic rotational spectrum is shown in Figures 3(a) and 4(a), while in Figures 3(b)–(c) and 4(b)–(c), we show the theoretical hyperfine patterns of the first two rotational transitions, $J = 1 \leftarrow J = 0$ and $J = 2 \leftarrow J = 1$ of NaNCO and NaOCN, respectively. For NaNCO, only the ^{23}Na nuclear quadrupole coupling hyperfine structure, which is spread over several MHz at very low frequencies, is included in the simulations. In the case of the NaOCN molecule the complex ^{14}N and ^{23}Na nuclear quadrupole coupling hyperfine structure is included in the predictions. Note that at higher frequencies, the hyperfine structure is expected to coalesce into observable line clusters of reinforced intensity, as seen for NaCl, whose hyperfine structure is not resolved in the millimeter-wave astronomical data (Cernicharo & Guélin 1987). At this point, the lack of available experimental information about the systems under study does not allow us to evaluate the accuracy of the frequency scale. Apart from recent theoretical studies reported

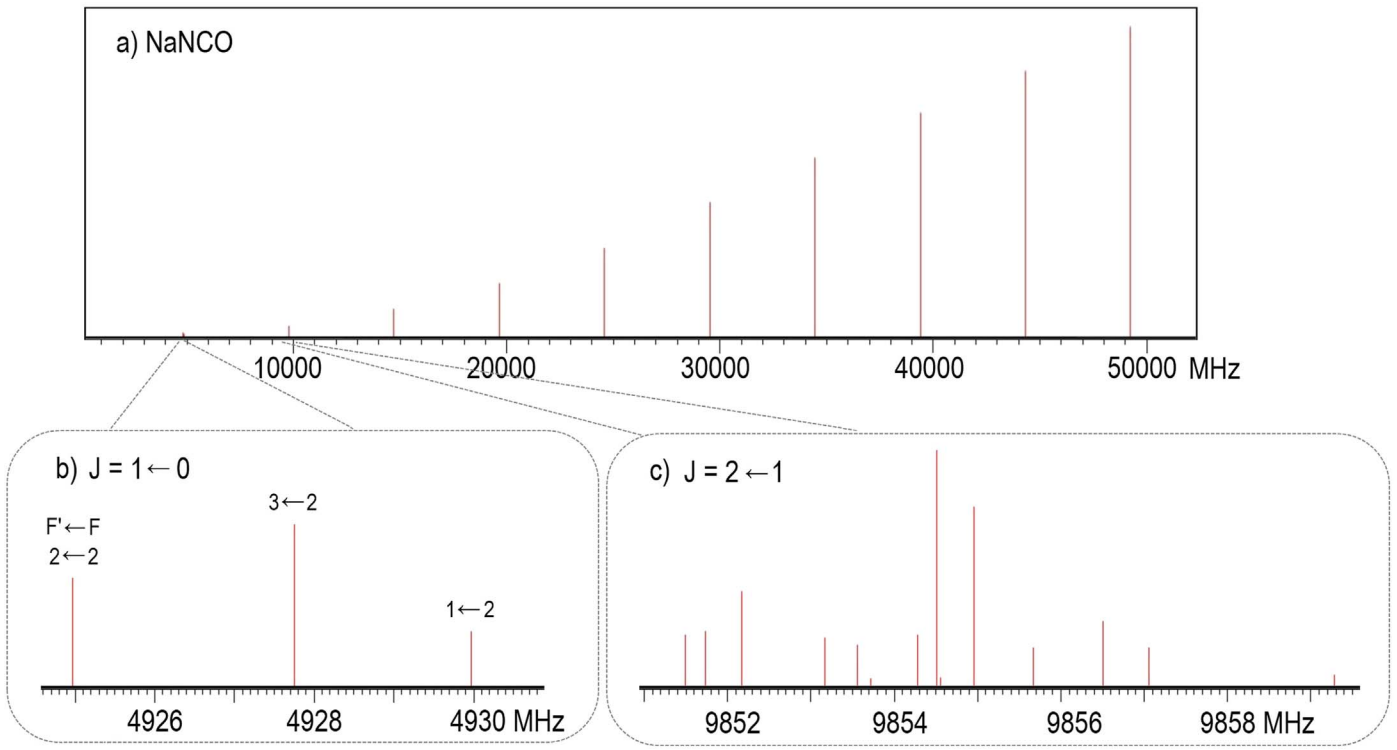

Figure 3. (a) Predicted synthetic rotational spectrum of linear NaNCO at 10 K in the 0–50 GHz frequency range, computed from the theoretical spectroscopic parameters listed in Table 4. (b) Zoomed view showing the $J = 1 \leftarrow 0$ transition of NaNCO. (c) Inset showing the more complex $J = 2 \leftarrow 1$ rotational transition of NaNCO. We employed a $^1\Sigma$ Hamiltonian in the following form: $H = H_R + H_Q$, where H_R includes rotational and centrifugal distortion parameters and H_Q considers the quadrupole coupling interaction. The energy levels involved in each transition are labeled with the quantum numbers J and F (F = J + I). Intensity is given in arbitrary units.

Table 6
Harmonic, ω, and Anharmonic, ν, Vibrational Frequencies (in cm^{-1}) and IR Intensities (in km/mol) computed at the CCSD(T,rw)/aug-cc-pVTZ level

NaNCO ($^1\Sigma$)					NaOCN ($^1\Sigma$)				
Mode	ω	I_{Harm}	ν	I_{Anh}	Mode	ω	I_{Harm}	ν	I_{Anh}
π NaNC bending	54	27.5	61	27.6	π NaOC bending	62	10.0	58	9.9
σ NaN stretching	377	69.4	380	66.9	σ NaO stretching	409	56.8	401	56.7
π NCO bending	645	11.1	642	10.3	π OCN bending	582	8.0	574	7.5
σ NCO sym stretching	1332	3.4	1313	3.3	σ OCN sym stretching	1234	164.1	1243	126.3
σ NCO asym stretching	2221	1113.5	2184	1051.7	σ OCN asym stretching	2246	488.0	2204	445.2

on this matter by Alessandrini et al. (2018), which estimate a deviation in the rest frequencies of ∼4 MHz for low-frequency centimeter wavelengths using related CC approaches, we can use the spectroscopic data for the related c-NaNC ($^1A'$) system (Van Vaals et al. 1984) to evaluate upper limit errors of ∼0.4%–0.7% in the values of the B and C rotational constants, when compared with CCSD(T,all)/aug-cc-pwCVQZ level predictions, only if we assume that the uncertainties are approximately transferable to our systems. This is translated in an uncertainty in the frequency scale of 19–34 MHz for NaNCO.

Finally, in Table 6 we provide the harmonic, ω, and anharmonic, ν, vibrational frequencies along with the corresponding infrared (IR) intensities for the lowest-lying isomers at the CCSD(T,rw)/aug-cc-pVTZ level to guide an eventual detection by means of IR spectroscopy. The IR spectrum of NaNCO is clearly dominated by an intense band related to the σ-NCO asymmetric stretching mode ($I_{Anh} = 1051.7$ km/mol). Following in intensity we find the σ-NaN stretching mode. Very similar features were reported for the related MgNCO (Vega-Vega et al. 2017). Similarly, the σ-NCO asymmetric stretching mode is the most prominent band in the IR spectrum of NaOCN ($I_{Anh} = 445.2$ km/mol), while the σ-NCO symmetric stretching mode is the second most intense band, in contrast to NaNCO. Moreover, if we analyze anharmonic contributions, which are often needed to model a reliable IR spectrum, we observe that for NaNCO, harmonic calculations of the lowest-frequency modes slightly underestimate fundamental frequencies while the contrary occurs for high-frequency modes. Overall, when comparing harmonic and anharmonic calculations, larger absolute differences are detected for high-frequency stretching modes. On the other hand, harmonic frequencies mostly overestimate fundamental frequencies for the sodium cyanate isomer. A final remark should be done about the low anharmonic frequencies of the bending modes for both NaNCO and NaOCN (61 and 58 cm^{-1}, respectively). These small values point to a floppy nature where both molecules shall undergo a large amplitude motion with

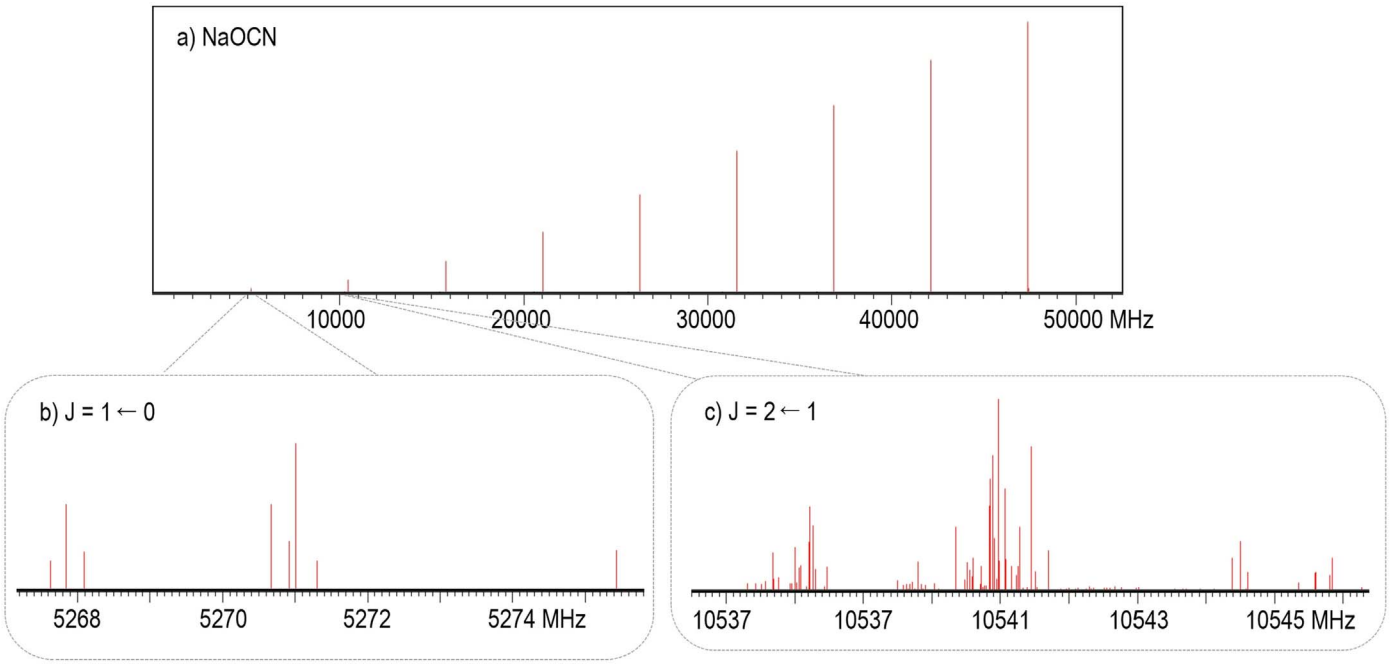

Figure 4. (a) Predicted synthetic rotational spectrum of quasilinear NaOCN at 10 K in the 0–50 GHz frequency range, computed from the theoretical spectroscopic parameters listed in Table 4. (b) Zoomed view showing the $J = 1 \leftarrow 0$ transition of NaOCN. (c) Zoomed view showing the $J = 2 \leftarrow 1$ transition of NaOCN.

respect to the aforementioned low-frequency modes. Moreover, these bending modes contribute significantly to the vibrational partition function. Hence, a vibrational correction factor is clearly needed to properly estimate line intensities at temperatures above 50 K and reproduce a trustworthy rotational spectrum.

Taken together, these theoretical spectroscopic data are mandatory to achieve an eventual laboratory detection and may even enable us to perform a first radio astronomical search. Although we anticipate a non-negligible uncertainty in the predicted rotational rest frequencies (see above), the high-level calculated hyperfine patterns of both NaNCO and NaOCN can be employed as a key pattern to characterize these molecules in a future microwave experimental study as well as, eventually, in space. In this regard, sensitive data at centimeter wavelengths, such as the new line spectral survey of IRC+10216 performed by Pardo et al. (2021b) might be directly tackled using the present theoretical information, trying to match any of the reported unidentified lines (U-lines) at the 5σ level or even some of the 50 features at the 3σ level with our predictions. Moreover, the high-level theoretical information provided here shall serve as a foundation for future theoretical methodologies.

4. Conclusions

With the improvement of modern observational facilities, there is a vast amount of new and very sensitive astronomical data, which is at an expense to be fully deciphered. In this regard, the synergy between radio astronomy and computational astrochemistry is lately helping to deal with some of the remaining unassigned spectral features. In this work we have studied the [Na, N, C, O] system using high-level computational methodologies. Nine different isomers have been identified toward the singlet ground-state potential energy surface and the interconversion and dissociation processes for the most relevant species have been analyzed. Sodium isocyanate, NaNCO, and sodium cyanate, NaONC, appears as the most promising targets to be searched for in the ISM, due to the tremendously high predicted electric dipole moment (11.4 and 13.6 D, respectively). Thus, we have provided a complete set of the relevant spectroscopic parameters needed to interpret their rotational spectra. The nuclear quadrupole hyperfine structure attributed to the presence of ^{23}Na and ^{14}N nuclei has been also predicted and analyzed. What is more, we report a theoretical vibrational study at the CCSD(T,rw)/aug-cc-pVTZ level, including anharmonic corrections. The predicted extremely bright intensity for the σ-NCO asymmetric stretching mode of NaNCO would greatly facilitate the detection of the NaNCO isomer in the ISM by IR spectroscopy. All in all, the present results will pave the route to their eventual laboratory characterization by means of rotational or IR spectroscopy, or even interstellar detection. Moreover, this information shall provide relevant insights into the chemistry of metal-bearing isocyanates/cyanates in space and, ultimately, the chemical pathways to their formation in space.

Financial support from the Spanish Ministerio de Ciencia e Innovación (PID2020-117742GB-I00) and Junta de Castilla y Leon (grant VA244P20) is gratefully acknowledged. P.O. acknowledges grant No. EDU/601/2020 (Junta de Castilla y Leon and European Social Fund).

Appendix

In Table A1 we list the experimental and computed structural parameters for the related c-NaNC (^{1}A′) as an additional theoretical benchmark.

Table A1
Structural Parameters for c-NaNC ($^1A'$) Computed at Different Levels of Theory Along with the Experimental Parameters Included for Comparison

Parameter[a]	Experimental[b]	B2PLYPD3/aug-cc-pVQZ	CCSD(T,rw)/aug-cc-pVTZ	CCSD(T,rw)/aug-cc-pVQZ	CCSD(T,rw)/aug-cc-pCV(T+d)Z	CCSD(T,rw)/aug-cc-pCV(Q+d)Z
r(Na-N)	2.233(15)	2.2373	2.1927	2.1078	2.16874	2.17485
r(N-C)	1.170(4)	1.1771	1.1841	1.1744	1.18413	1.18042
r(Na-C)	2.379(15)	2.3915	2.3433	1.9573	2.3209	2.31993

Parameter	CCSD(T,rw)/aug-cc-pCV(5+d)Z	CCSD(T,all)/cc-pwCVQZ	CCSD(T,all)/aug-cc-pwCVQZ	CCSD(T,rw)-F12/cc-pCVTZ-F12	CCSD(T,rw)-F12/cc-pCVQZ-F12
r(Na-N)	2.2042	2.2226	2.2233	2.22536	2.2193
r(N-C)	1.1803	1.1781	1.1785	1.1806	1.1818
r(Na-C)	2.3588	2.3726	2.3740	2.37554	2.3792

Notes.
[a] Bond distances are given in angstroms;
[b] Experimental parameters from a high-resolution molecular beam spectroscopic study by Van Vaals et al. (1984).

ORCID iDs

Miguel Sanz-Novo https://orcid.org/0000-0001-9629-0257
Pablo Ortega https://orcid.org/0000-0003-2480-6220
Pilar Redondo https://orcid.org/0000-0001-7876-4818
Antonio Largo https://orcid.org/0000-0003-4959-4850
José Luis Alonso https://orcid.org/0000-0002-3146-8250
Carmen Barrientos https://orcid.org/0000-0003-0078-7379

References

Alessandrini, S., Gauss, J., & Puzzarini, C. 2018, J. Chem. Theory Comput., 14, 5360
Bai, J., & Yu, H.-T. 2022, New J. Chem., 46, 7879
Barone, V. 2005, JChPh, 122, 014108
Belloche, A., Garrod, R. T., Müller, H. S. P., et al. 2019, A&A, 628, A10
Belloche, A., Meshcheryakov, A. A., Garrod, R. T., et al. 2017, A&A, 601, A49
Bisschop, S. E., Jørgensen, J. K., van Dishoeck, E. F., & de Wachter, E. B. M. 2007, A&A, 465, 913
Brünken, S., Belloche, A., Martín, S., Verheyen, L., & Menten, K. M. 2010, A&A, 516, A109
Cabezas, C., Barrientos, C., Largo, A., et al. 2014, JChPh, 141, 104305
Cabezas, C., Cernicharo, J., Alonso, J. L., et al. 2013, ApJ, 775, 133
Canelo, C. M., Bronfman, L., Mendoza, E., et al. 2021, MNRAS, 504, 4428
Cernicharo, J., Agúndez, M., Cabezas, C., et al. 2021, A&A, 656, L21
Cernicharo, J., Cabezas, C., Pardo, J. R., et al. 2019b, A&A, 630, L2
Cernicharo, J., & Guélin, M. 1987, A&A, 183, L10
Cernicharo, J., Kisiel, Z., Tercero, B., et al. 2016, A&A, 587, L4
Cernicharo, J., Velilla-Prieto, L., Agúndez, M., et al. 2019a, A&A, 627, L4
Colzi, L., Rivilla, V. M., Beltrán, M. T., et al. 2021, A&A, 653, A129
Csengeri, T., Belloche, A., Bontemps, S., et al. 2019, A&A, 632, A57
Dunning, T. H. 1989, JChPh, 90, 1007
Ellingboe, L. C., Bopegedera, A. M. R. P., Brazier, C. R., & Bernath, P. F. 1986, CPL, 126, 285
Frisch, M. J., Trucks, G. W., Schlegel, H. B., et al. 2016, Gaussian 16, Revision B+01 (Wallingford, CT: Gaussian)
Gonzalez, C., & Schlegel, H. B. 1989, JChPh, 90, 2154
Gonzalez, C., & Schlegel, H. B. 1990, JChPh, 94, 5523
Gorai, P., Bhat, B., Sil, M., et al. 2020, ApJ, 895, 86
Gordy, W., & Cook, R. L. 1984, Microwave Molecular Spectra (3rd edn.; New York: Wiley)
Grimme, S. J. 2006, ChPh, 124, 034108
Guélin, M., Lucas, R., & Cernicharo, J. 1993, A&A, 280, L19
Guélin, M., Muller, S., Cernicharo, J., et al. 2000, A&A, 363, L9
Guélin, M., Muller, S., Cernicharo, J., et al. 2004, A&A, 426, L49
Gupta, H., Gottlieb, C. A., Lattanzi, V., et al. 2013, ApJL, 778, L1
Halfen, D., Ilyushin, V. V., & Ziurys, L. M. 2015, ApJ, 812, L5
Helmich, F. P., & van Dishoeck, E. F. 1997, A&AS, 124, 205
Highberger, J. L., Savage, C., Bieging, J. H., & Ziurys, L. M. 2001, ApJ, 562, 790
Hill, J. G., & Peterson, K. A. 2017, JPhCh, 147, 244106
Hollis, J. M., Lovas, F. J., Remijan, A. J., et al. 2006, ApJ, 643, L25
Hollis, J. M., & Rhodes, P. J. 1982, ApJ, 262, L1
Jackson, J. M., Armstrong, J. T., & Barrett, A. H. 1984, ApJ, 280, 608
Jiang, W., DeYonker, N. J., & Wilson, A. K. 2012, JCTC, 8, 460
Jiménez-Serra, I., Martín-Pintado, J., Rivilla, V. M., et al. 2020, AsBio, 20, 1048
Kawaguchi, K., Kagi, E., Hirano, T., et al. 1993, ApJL, 406, L39
Kawaguchi, K., Kasai, Y., Ishikawa, S., & Kaifu, N. 1995, PASJ, 47, 853
Knizia, G., Adler, T. B., & Werner, H.-J. 2009, JChPh, 130, 054104
Lee, T. J., & Taylor, P. R. 1989, IJQC, 36, 199
Ligterink, N. F. W., Ahmadi, A., Coutens, A., et al. 2021, A&A, 647, A87
Ligterink, N. F. W., Ahmadi, A., Luitel, B., et al. 2022, ESC, 6, 455
Ligterink, N. F. W., Coutens, A., Kofman, V., et al. 2017, MNRAS, 469, 2219
Ligterink, N. F. W., El-Abd, S. J., Brogan, C. L., et al. 2020, ApJ, 901, 37
Manigand, S., Jørgensen, J. K., Calcutt, H., et al. 2020, A&A, 635, A48
Marcelino, N., Agúndez, M., Cernicharo, J., Roueff, E., & Tafalla, M. 2018, A&A, 612, L10
Marcelino, N., Brünken, S., Cernicharo, J., et al. 2010, A&A, 516, A105
Marcelino, N., Cernicharo, J., Tercero, B., & Roueff, E. 2009, ApJL, 690, L27
Martín-Doménech, R., Rivilla, V., Jiménez-Serra, I., et al. 2017, MNRAS, 469, 2230
McCarthy, M. C., & McGuire, B. A. 2021, JPCA, 125, 3231
McGuire, B. A. 2018, ApJS, 239, 17
McGuire, B. A., Burkhardt, A. M., Loomis, R. A., et al. 2020, ApJL, 900, L10
Mills, I. M. 1972 (Vibration-Rotation Structure in Asymmetric and Symmetric-Top Molecules. In Molecular Spectroscopy: Modern Research) ed. K. N. Rao & C. W. Mathews (New York: Academic Press), 115
Mladenovic, M., & Lewerenz, M. 2008, CP, 343, 129
Nazari, P., van Gelder, M. L., van Dishoeck, E. F., et al. 2021, A&A, 650, A150
Nguyen-Q-Rieu, Henkel, C., Jackson, J. M., & Mauersberger, R. 1991, A&A, 241, L33
Pardo, J. R., Cabezas, C., Fonfría, J. P., et al. 2021a, A&A, 652, L13
Pardo, J. R., Cernicharo, J., Tercero, B., et al. 2021b, A&A, 658, A39
Pascal, R., Boiteau, L., Commeyras, A., et al. 2005, in From the Prebiotic Synthesis of α-Amino Acids Towards a Primitive Translation Apparatus for the Synthesis of Peptides, ed. P. Walde (Berlin: Springer), 69
Pasinszki, T., Veszprémi, T., & Fehér, M. 1993, CPL, 215, 395
Peterson, K. A., Adler, T. B., & Werner, H. J. 2008, JChPh, 128, 084102
Pickett, H. M. 1991, JMoSp, 148, 371
Pickett, H. M., Poynter, R. L., Cohen, E. A., et al. 1998, JQSRT, 60, 883
Poppinger, D., & Radom, L. J. 1978, JAChS, 100, 3674
Pulliam, R. L., Savage, C., Agúndez, M., et al. 2010, ApJL, 725, L181
Raghavachari, K., Trucks, G. W., Pople, J. A., & Head-Gordon, M. 1989, CPL, 157, 479
Redondo, P., Barrientos, C., & Largo, A. 2016, ApJ, 828, 45
Redondo, P., Barrientos, C., & Largo, A. 2019, ApJ, 871, 180
Redondo, P., Largo, A., & Barrientos, C. 2020, ApJ, 899, 135
Redondo, P., Largo, A., Vega-Vega, A., & Barrientos, C. 2015, JChPh, 142, 184301
Redondo, P., Sanz-Novo, M., & Barrientos, C. 2022, ApJ, 928, 69
Rivilla, V. M., Jiménez-Serra, I., Martín-Pintado, J., et al. 2021, PNAS, 118, e2101314118
Rode, B. M., Kosmus, W., & Nachbaur, E. 1972, CPL, 17, 186
Rodríguez-Almeida, L. F., Rivilla, V. M., Jiménez-Serra, I., et al. 2021, A&A, 654, L1

Rodríguez-Fernández, N. J., Tafalla, M., Gueth, F., & Bachiller, R. 2010, A&A, 516, A98
Sanz, M. E., McCarthy, M. C., & Thaddeus, P. 2002, ApJL, 577, L71
Sanz-Novo, M., León, I., Alonso, J. L., Largo, A., & Barrientos, C. 2020, A&A, 644, A3
Schwabe, T., & Grimme, S. 2007, PCCP, 9, 3397
Snyder, L. E., & Buhl, D. 1972, ApJ, 177, 619
Stanton, J. F., Gauss, J., Harding, M. E., & Szalay, P. G. 2013, CFOUR, A Quantum Chemical Program, http://www.cfour.de/
Sun, M., Apponi, A. J., & Ziurys, L. M. 2009, JChPh, 130, 034309
Trabelsi, T., Davis, M. C., Fortenberry, R. C., & Francisco, J. S. 2019, JChPh, 151, 244303
Turner, B. E. 1991, ApJ, 376, 573
Turner, B. E., Steimle, T. C., & Meerts, L. 1994, ApJL, 426, L97
Turner, B. E., Terzieva, R., & Herbst, E. 1999, ApJ, 518, 699
Van Vaals, J. J., Meerts, W. L., & Dymanus, A. 1984, CP, 86, 147
Vega-Vega, A., Largo, P., & Redondo, C. 2017, ECS, 1, 158
Veszprémi, T., Pasinszki, T., & Fehér, M. 1994, JAChS, 116, 6303
Werner, H.-J., & Knowles, P. J. 1985a, JChPh, 82, 5053
Werner, H.-J., & Knowles, P. J. 1985b, CPL, 115, 259
Werner, H.-J., Knowles, P. J., Knizia, G., et al. 2019, MOLPRO, v2020.1, https://www.molpro.net/
Woon, D. E., & Dunning, T. H. 1993, JChPh, 98, 1358
Yamada, K. J. Mol. 1980, JMoSp, 79, 323
Zack, L. N., Halfen, D. T., & Ziurys, L. M. 2011, ApJL, 733, L36
Zeng, S., Jiménez-Serra, I., Rivilla, V. M., et al. 2018, MNRAS, 478, 2962
Ziurys, L. M., Apponi, A. J., Guélin, M., & Cernicharo, J. 1995, ApJL, 445, L47
Ziurys, L. M., Savage, C., Highberger, J. L., et al. 2002, ApJL, 564, L45